Journal of Controlled Release 367 (2024) 697–707

Contents lists available at ScienceDirect

Journal of Controlled Release

journal homepage: www.elsevier.com/locate/jconrel

Genetically engineered macrophages as living cell drug carriers for targeted cancer therapy

Pengbo Ning [a,b,*,1], Fuyu Du [a,b,1], Haotian Wang [c,1], Xiaocheng Gong [a,b], Yuqiong Xia [a,b], Xianghan Zhang [a,b], Hongzhang Deng [a,b], Ruili Zhang [a,b,*], Zhongliang Wang [a,b,*]

[a] School of Life Science and Technology, Xidian University, Xi'an, Shaanxi 710071, PR China
[b] Engineering Research Center of Molecular & Neuroimaging, Ministry of Education, Xi'an, Shaanxi 710071, PR China
[c] Department of radiology, Cancer Hospital of China Medical University, Liaoning Cancer Hospital and Institute, Shenyang, Liaoning 110801, China

ARTICLE INFO

Keywords:
Engineering macrophages
Targeting therapy
Nano delivery
Solid tumor
HER2

ABSTRACT

Precise targeting is a major prerequisite for effective cancer therapy because it ensures a sufficient therapeutic dosage in tumors while minimizing off-target side effects. Herein, we report a live-macrophage-based therapeutic system for high-efficiency tumor therapy. As a proof of concept, anti-human epidermal growth factor receptor-2 (HER2) affibodies were genetically engineered onto the extracellular membrane of macrophages (AE-Mφ), which further internalized doxorubicin (DOX)-loaded poly(lactic-*co*-glycolic acid) nanoparticles (NPs) to produce a macrophage-based therapeutic system armed with anti-HER2 affibodies. NPs(DOX)@AE-Mφ were able to target HER2+ cancer cells and specifically elicit affibody-mediated cell therapy. Most importantly, the superior HER2 + -targeting capability of NPs(DOX)@AE-Mφ greatly guaranteed high accumulation at the tumor site for improved chemotherapy, which acted synergistically with cell therapy to significantly enhance anti-tumor efficacy. This study suggests that NPs(DOX)@AE-Mφ could be utilized as an innovative 'living targeted drug' platform for combining both macrophage-mediated cell therapy and targeted chemotherapy for the individualized treatment of solid tumors.

1. Introduction

The lack of targeted delivery of therapeutic drugs is a major obstacle in developing potent cancer therapies with minimal off-target side effects on normal tissues [1–3]. To address this issue, much effort has been devoted to formulating various targeted delivery systems, such as nano-enabled drug delivery systems, antibody-drug conjugates, and biomimetic delivery vehicles [4–7]. Among them, nature-inspired biomimetic vehicles have attracted substantial attention in recent years [8]. By leveraging erythrocytes, platelets, immune cells, cancer cells, cell-derived membranes, or extracellular vesicles, biomimetic vehicles can closely mimic the key structural and biological attributes of natural circulatory carriers [9–12], thereby showing improved biocompatibility, prolonged blood circulation, immune evasion, and, in some cases, intrinsic disease-targeting capability.

As one of the most abundant immune cells in the tumor microenvironment, macrophages are highly attractive candidates for therapeutic drug delivery. They share favorable features with other cells and also possess natural tumor-homing ability and intrinsic phagocytic capability, which enables them to internalize considerable drug loads and directionally deliver the drugs to the tumor site [5,13,14]. Several drug delivery systems using macrophages and macrophage membranes have been reported to improve therapeutic effects [15–17]. However, most of these systems utilize only the inherent tumor tropism of macrophages to migrate towards tumor sites, leading to insufficient targeting ability. Although straightforward chemical conjugation has been widely used to introduce exogenous tumor-targeting motifs (e.g., small molecules, peptides, and antibodies) on macrophage surfaces [18,19], a number of issues need to be addressed, including, but not limited to, the chemical toxicity of macrophages, tedious conjugation process, prevailing membrane protein denaturation, and unpredictable binding sites [20,21]. These issues often negatively impact targeting efficiency and pose additional challenges for the translation of macrophage-based delivery systems into clinical practice. Consequently, it remains a formidable challenge to develop living macrophage-based vehicles that can ferry therapeutic drugs specifically to their sites of action with improved

* Corresponding authors at: School of Life Science and Technology, Xidian University, Xi'an, Shaanxi 710071, PR China.
E-mail addresses: pbning@xidian.edu.cn (P. Ning), rlzhang@xidian.edu.cn (R. Zhang), wangzl@xidian.edu.cn (Z. Wang).
[1] These authors contributed equally to this work.

https://doi.org/10.1016/j.jconrel.2024.02.003
Received 10 September 2023; Received in revised form 3 February 2024; Accepted 5 February 2024
Available online 9 February 2024

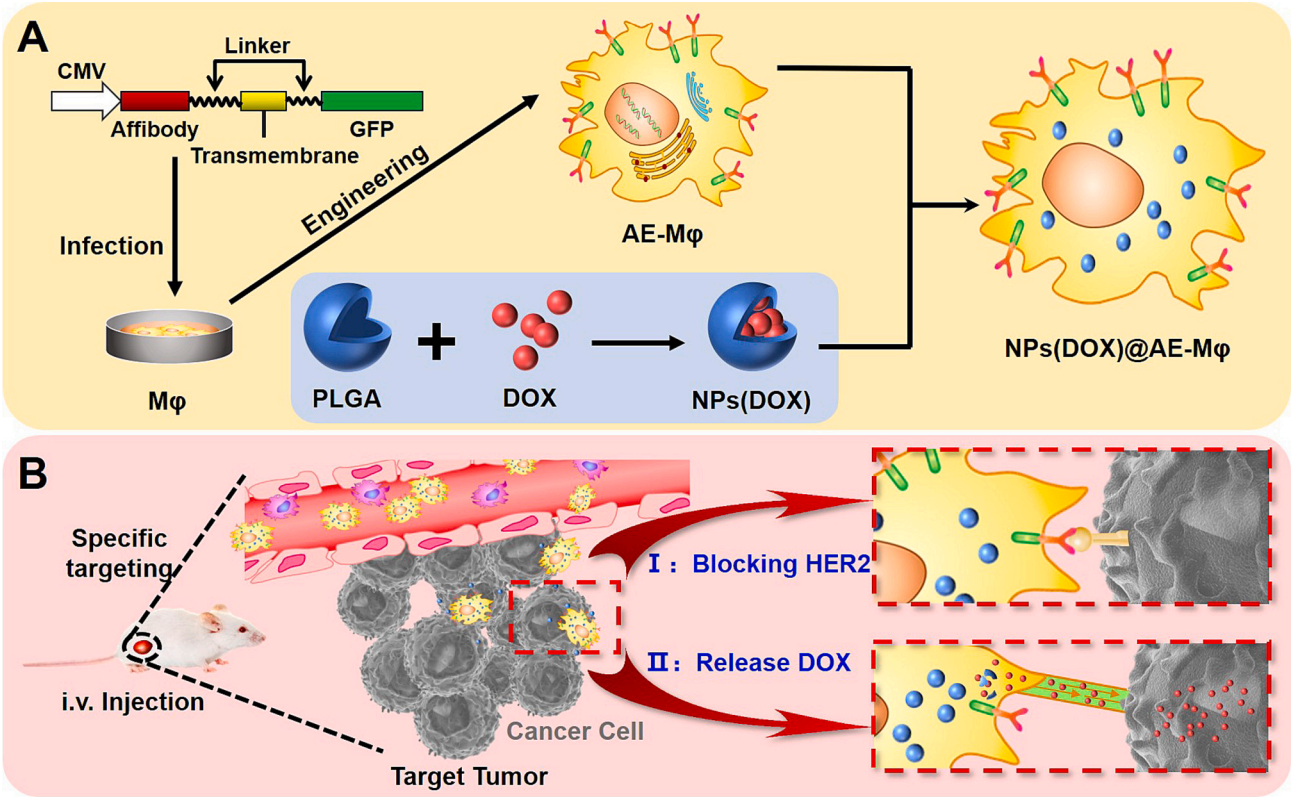

Scheme 1. Schematic illustration of engineering macrophages as a "living targeted drug" technology platform
(A) The specific gene sequence, including the anti-HER2+ antibody, was integrated into the genome of macrophages. The anti-HER2+ antibody would be anchored on the cell surface to inform engineering macrophages. NPs (DOX) were prepared and then loaded into engineering macrophages. (B) Engineering macrophages with anti-HER2+ antibodies can specifically bind to the HER2 of tumor cells to inhibit tumor growth. Meanwhile, the engineering macrophages facilitate chemotherapy drug delivery to solid tumors based on their specific targeting ability.

targeting ability [22].

Unlike post-fabrication approaches that incorporate extra functionality, genome editing allows for a flexible design to produce new cell lines with specific targeting properties, stable modifications, long-term effects, and ultimately, enhanced therapeutic efficacy [23,24]. With advances in synthetic biology and the successful clinical application of chimeric antigen receptor T-cells (CAR-T), genetic cell engineering has emerged as a promising strategy for diverse biomedical applications [25,26]. Therefore, we envisioned that introducing targeting moieties into macrophages through genetic engineering would facilitate their homing to tumors with enhanced targeting abilities. Nevertheless, treatments involving a single therapeutic modality (monotherapy) are often insufficient to kill tumor cells effectively [27]. Ideally, the development of a macrophage-based therapeutic system capable of specifically targeting tumors and exerting multimodal tumoricidal effects would be preferable in cancer treatment.

Herein, we report a robust method to provide genetically engineered macrophages as live cell therapeutics for both tumor-targeting and synergistic tumor therapy (Scheme 1). As a proof of concept, human epidermal growth factor receptor 2 (HER2)-positive breast cancer cells were used to demonstrate the effectiveness of our strategy. Specifically, anti-HER2 affibodies were stably transmembrane-expressed on the extracellular membranes of macrophages to generate affibody-armed engineered macrophages (AE-Mφ). Doxorubicin (DOX), a model small molecule anti-cancer drug, was encapsulated into poly (lactic-*co*-glycolic acid) (PLGA) to form nanoparticles (NPs (DOX)), followed by macrophage internalization to produce macrophage-based delivery vehicles, NPs (DOX)@AE-Mφ. Benefiting from the armed extracellular anti-HER2 antibody domain on the surface, NPs (DOX)@AE-Mφ exhibit high specificity and affinity towards $HER2^{+}$ tumor cells. This could enable the targeted delivery of encapsulated DOX@PLGA to the tumor site for enhanced tumor chemotherapy, and effectively block the intracellular HER2 signaling pathway to induce considerable cytotoxicity. The highly targeted antibody-mediated therapy and chemotherapy act synergistically to elicit amplified therapeutic efficacy against tumor growth. Our results indicate that NPs (DOX)@AE-Mφ could serve as a promising cancer-targeting platform for enhancing cancer therapeutic efficacy by overcoming limitations in drug delivery and cancer treatment.

2. Materials and methods

2.1. Cell culture

DMEM/HIGH GLUCOSE (hyclone) was used to sustain mouse macrophage RAW264.7 or human breast cancer cell line MDA-MB-453, whilst RPMI-1640 (hyclone) was used to grow mouse breast cancer cells. Both media included 10% fetal bovine serum (FBS, GIBCO). MDA-MB-453 cells were cultivated at 37 °C with 100% air, whereas RAW264.7 or 4 T1 cells were done so in an environment that included 5% CO_2.

2.2. Plasmid construction

Shanghai Generay Biotech Co., Ltd. (http://www.generay.com.cn/) created the Sig-affibody-GFP sequence, and YouBio (http://www.youbio.cn/) provided the pCDH-CMV-MCS-EF1-Puro. After that, enzymatic digestion was used to create the recombinant plasmid that included the target DNA fragment.

2.3. Construction of lentivirus

Synthesized and cloned into a third-generation lentiviral plasmid were designed CAR-like constructs. Each sequence of the signal peptide, affibody, transmembrane domain, and GFP was the same in all CAR-like constructs. In a nutshell, day 0 activation of 293 T cells was followed by culture in DMEM high-glucose media with 10% FBS. On day 1, the lentiviral system's shuttle plasmid and helper plasmid were co-incubated before the combination was injected into 293 T cells using the TurboFect Transfection Reagent. Cells were packaged with lentivirus on day 3 until it was discovered that there was enough GFP fluorescence to sustain the production of lentiviral particles [28]. The lentivirus product was concentrated and purified before being placed in liquid nitrogen to await functional testing.

2.4. Quantitative polymerase chain reaction (qPCR)

Quantitative PCR was used to evaluate relative mRNA expression. These were the GFP primers that were used: 5-ACGACGGCAECTACAE-GACC-3 and 5-TTGTACTCCAGCTTGTGCCC-3′. The $2^{-\Delta\Delta Ct}$ technique was utilized to determine the relative expression levels during the triplicate qPCR analysis.

2.5. Western blot analysis

Western blotting was used to quantify the expression of the Affibody-GFP protein. SDS-PAGE was used to separate the total protein extracts from the Pageruler protein ladder (Thermo Fisher, #26616), which was then transferred to Immobilon-P membranes (Millipore, Billerica, Massachusetts, USA). The membranes were first blocked in TBST buffer for 1 h, and then overnight at 4 °C, they were treated with primary rabbit monoclonal anti-GFP antibody diluted in TBST (1:1000; omnimabs). Six times for a total of five min, anti-GFP antibody was withdrawn and washed in TBST. After diluting the secondary antibody by 1/5000 in TBST solution, the membrane was incubated there for 1 h. An ECL detection procedure was carried out using a GeneGnome XRQ Chemiluminescence Detector (Syngene, Cambridge, UK) after the membrane had been cleaned with TBST buffer.

2.6. Flow cytometry

RAW264.7 and Sig-Affibody-Mφ (4×10^5) cells were plated onto 6-well dishes and grown at 37 °C with 5% CO_2 in an incubator. Next, 100 μL of HER2 protein labeled with PE dye (1 mg/mL, Abiocenter) was added to the DMEM culture medium and incubated with Sig-Affibody-Mφ and RAW264.7 cells for 4–6 h. The cells were digested by trypsin, centrifuged at 1000 rpm, 4 °C for 3 min, washed 2–3 times with PBS, and resuspended in 200 μL PBS. FACSCalibur flow cytometry (BD Biosciences) and Cell Quest software (BD Biosciences) were used for analysis.

2.7. Affibody binding activity assay

RAW264.7 and Sig-Affibody-Mφ cells were plated into 12-well dishes, co-cultured with HER2-PE for 4–6 h, and then three times with PBS washed. After being fixed for 20–30 min with 4% paraformaldehyde, the cell samples were washed three times in PBS. The cells were examined using a Leica fluorescence microscope after the nuclei were stained with DAPI for 10–15 min.

2.8. Co-immunoprecipitation (CO-IP) assay

To verify the specific binding activity of Sig-Affibody-Mφ to HER2, CO-IP assays were carried out. First, 5×10^5 RAW264.7 cells and Sig-Affibody-Mφ were seeded in 6-well culture plate with 1 mL DMEM/HIGH GLUCOSE. After 24 h, 200 μL HER2 recombinant protein (0.1 mg/mL) was added and incubated with RAW264.7, and Sig-Affibody-Mφ for 4 h. The cells were then washed three times with PBS to remove unbound HER2 recombinant protein. Next, the cells were lysed in 300 μL RIPA lysis buffer (HAT) containing 1% PSMF and protease inhibitor. The cell lysate was centrifugated at 12,000 × rpm for 15 min at 4 °C. The collected protein samples were verified by immunocoprecipitation test with PierceTM CO-Immunoprecipitation Kit (26,149, Thermofisher), and the specific operation steps were strictly in accordance with the manufacturer's instructions. The bound proteins were subjected to 10% SDS-PAGE and western blot analysis.

2.9. Preparation of PLGA-DOX nanoparticles

An oil-in-water emulsion solvent evaporation method was used [29]. In brief, 10 mg PLGA and 1 mg DOX were solubilized in 1 mL dichloromethane, and then the organic phase was added to 8 mL 2% PVA solution and sonicated for 4 min at 150 W in iced water. Next, vacuum depression vaporization was used to remove organic material [30]. The nanoparticles were centrifuged for 20 min at 15,000 rpm. The PLGA-DOX NPs were washed three times with purified water. The concentration of DOX encapsulated in the NPs was measured using a UV spectrophotometer [31].

2.10. Cell counting kit-8 (CCK8) analysis

1×10^4 MDA-MB-453 cells were added to 100 μL of DMEM/HIGH GLUCOSE medium with 10% FBS in 96-well plates (Corning). After being cultured for 24 h, 100 μL of RAW264.7, Sig-Affibody-Mφ, PLGA-DOX@RAW264.7, and PLGA-DOX@Sig-Affibody-Mφ were added to 96-well plates respectively, and the E:T ratios were 0:1, 0.25:1, 0.5:1, 0.75:1, 1:1, respectively. Effector(E) and tumor(T) cells were co-cultured for 48 h in 96-well plates at the indicated E:T ratios. After 2 days, the number of viable cells was determined using the Cell Counting kit-8 (CCK8, Dojindo Molecular Technologies).

2.11. Cell viability assays

Cell viability assays were carried out using a real-time cell analyzer (RTCA; xCELLigence, Roche Diagnostics K. K.) in real time. The system measures electrical impedance at the bottom of the tissue culture *E*-plates, which contains interdigitated electrodes, as the cell index. Human breast cancer cell MDA-MB-453 was seeded on *E*-plate 16 at 1×10^4 cells per well and precultured for 12–24 h. Effector cells RAW264.7, Sig-Affibody-Mφ, PLGA-DOX@RAW264.7 and PLGA-DOX@Sig-Affibody-Mφ were added with target ratio of 0:1, 0.25:1, 0.5:1, 0.75:1, 1:1, respectively. At the same time, we seeded the same amount of effector cells into E-Plate 16 without tumor cells. Cell viability was monitored by RTCA for 48–72 h.

2.12. Construction of $HER2^+$ 4 T1 cell

4 T1 cells in RPMI 1640 containing 10% FBS were cultured in six-well dishes. A HER2 cDNA expression plasmid (HG10004-ACGLN) was obtained from Sino Biological Inc., US, for constructing $HER2^+$ lentiviruses. Then, 4 T1 cells were transfected with $HER2^+$ lentivirus in accordance with the manufacturer's instructions. At 48 h after transfection with the lentivirus, $HER2^+$ 4 T1 cells were collected to establish a $HER2^+$ 4 T1 tumor model in mice. Meanwhile, qRT-PCR analysis of HER2 and GFP fluorescence testing was carried out to ensure that HER2 was successfully expressed in 4 T1 cells.

2.13. Mouse systemic tumor model

Four- to six-week-old BALB/c mice were obtained from Tengxin Biotechnology (Chongqing, China, http://www.cqtx123.com/), according to all relevant animal use guidelines and ethical regulations. A

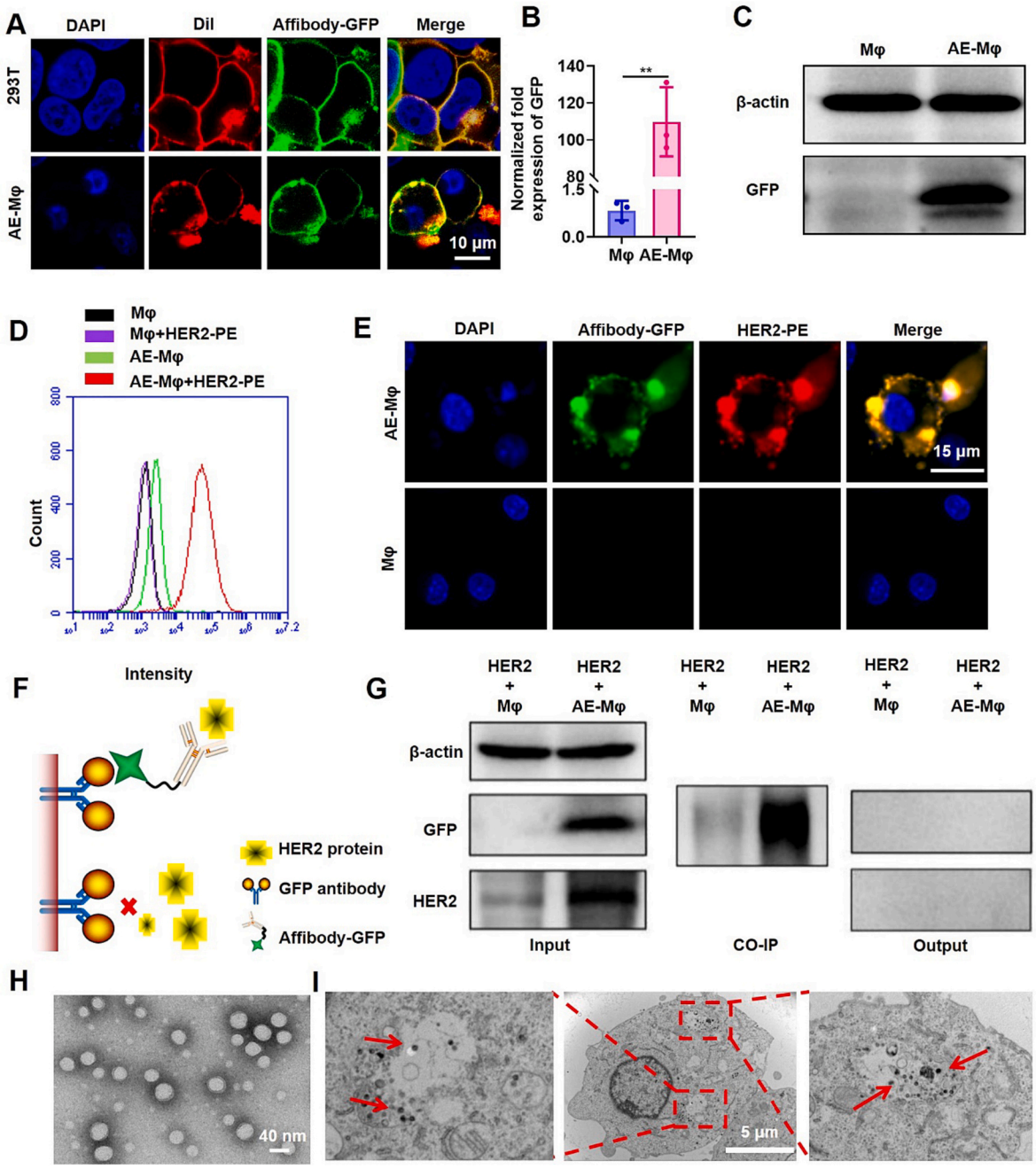

Fig. 1. Bioactive HER2 binding ability of affibody-armed macrophages in vitro. (A) The confocal imaging of affibody-armed engineering macrophages (AE-Mφ), expressing anti-HER2 domain. The specific gene sequence including anti-HER2+ affibody, transmembrane protein and GFP was cloned into lentivirus vector pLV, which was transfected into macrophages and then expressed the effector protein secreted to cells. The results showed that the green fluorescence (affibody-GFP) overlaped with the red fluorescence (DiI dye), which demonstrated the transmembrane localization of affibody-GFP. (B) The expression of affbody-GFP was verified by qRT-PCR analysis at the level of transcription. The data are presented as means ± SD, ** represents $P < 0.01$. (C) The expression of affbody-GFP was verified by Western Blot analysis at the level of translation. AE-Mφ was compared with RAW264.7 macrophage (Mφ) in which β-actin was used for standardization for each sample. (D) The representative flow cytometric analysis images of HER2-PE binding with AE-Mφ. HER2 recombinant protein labeled with PE dye (HER2-PE) or PBS was incubated with AE-Mφ as indicated. (E) Confocal scanning analysis indicated HER2-PE bound on the cell membrane of AE-Mφ. HER-PE (Red) was incubated with AE-Mφ or Mφ. Green fluorescent protein was conjugated to affibody molecule for indicating its localization on cell membrane. (F) CO-IP and western blotting technology were used to examine the interaction between HER2-PE (recombinant protein) and Affibody (armed on AE-Mφ). (G) HER2 protein was incubated with A*E*-Mφ or Mφ to obtain the input sample. The eluent products as CO-IP samples of AE-Mφ immunoprecipitated along with anti-GFP indicates a direct interaction between AE-Mφ and anti-GFP antibody with the commercial resin column, No protein were found on the output samples. (H) Characterization of TEM of PLGA(DOX) nanoparticles. (I) Characterization of TME after AE-Mφ phagocytosis of PLGA(DOX) nanoparticles. (For interpretation of the references to colour in this figure legend, the reader is referred to the web version of this article.)

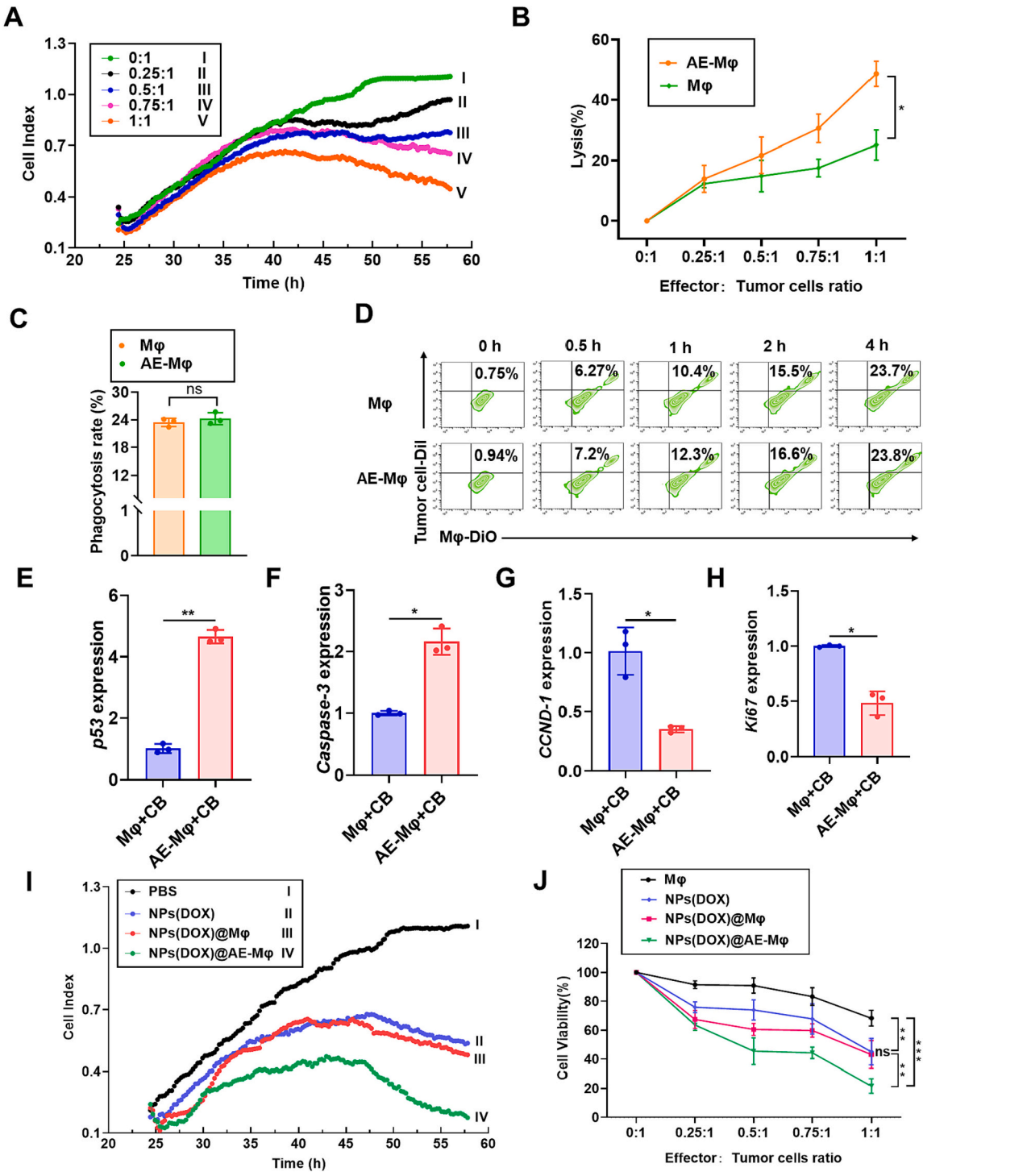

Fig. 2. The confirmed anti-tumor bioactivity on affibody-armed macrophages in vitro while drug-loading affibody-armed macrophages exhibited significant enhanced anti-tumor efficacy. (A) Affibody-armed macrophages (AE-Mφ) carry out anti-tumor bioactivity to MDA-MB-453 ($HER2^{+}$) cells with increased E:T ratio. (B) Cytotoxicity was assayed by measuring the amount of lactate dehydrogenase (LDH) released into cultured media. Error bars represent SD, $n = 3$, $^{*}P < 0.05$, $^{**}P < 0.01$, $^{***}P < 0.001$. AE-Mφ or RAW264.7 (Mφ) was incubated with MDA-MB-453 (HER2+) with increased E:T ratio. (C) There is no significant difference on phagocytosis ability between AE-Mφ and Mφ group. (D) Time-dependent phagocytosis was demonstrated by flow cytometry analysis, which indicated it is armed affibody that significantly contributed to enhanced cytotoxicity of AE-Mφ. (E) Key gene *p53* was detected after MDA-MB-453 cells were treated with affibody. AE-Mφ + CB and Mφ + CB group lose the phagocytosis function and only the role of affibody is retained. (F) The *Caspase-3* was detected after MDA-MB-453 cells were treated with affibody. (G) The *CCND-1* was detected after MDA-MB-453 cells were treated with affibody. (H) The *Ki67* was detected after MDA-MB-453 cells were treated with affibody. (I) NPs(DOX)@AE-Mφ and NPs(DOX)@Mφ were incubated with MDA-MB-453 cells, respectively. A growth curve of MDA-MB-453 cells was measured using a RT-CES system, which showed the drug loading affibody-armed macrophages had higher killing effects than those of drug delivery of conventional macrophages. NPs(DOX) and PBS groups were set as the control. (J) Comparison of cytotoxicity in vitro among NPs(DOX)@AE-Mφ, NPs(DOX)@Mφ, NPs(DOX) and Mφ groups by CCK8 analysis. The best anti-tumor effect was achieved in the NPs(DOX)@AE-Mφ group with increased E:T ratio. *, ** and *** represent $P < 0.05$, $P < 0.01$ and $P < 0.001$, respectively.

total of 5 × 10^6 $Her2^+$-4 T1 cells were administered to each mouse to establish a subcutaneous tumor model. Seven days later, 2 × 10^6 macrophages were administered intravenously via the tail vein (0 h) to carry out the targeting test. Tumor burden was recorded by bioluminescence imaging with a live animal imaging system (IVIS Lumina III, US) at 0 h, 2 h, 4 h, 8 h, 12 h, 24 h, and 48 h. Living Image software (Lumina) was used to analyze acquired bioluminescence data. Different therapeutic schedules were performed on other tumor-bearing mice, randomized into PBS, RAW, Sig-Affibody-Mφ, and PLGA-DOX@Sig-Affibody-Mφ group (n = 3). Next, 1 × 10^6 RAW264.7, Sig-Affibody-Mφ, and PLGA-DOX@Sig-Affibody-Mφ cells were administered intratumorally around the tumor in BALB/c mice. Subsequently, RAW264.7, Sig-Affibody-Mφ, and PLGA-DOX@Sig-Affibody-Mφ cells were injected every 2 days and seven times in total, and tumor volume and mouse weight were measured every 2 days. In terms of tail vein administration, two-time treatments were administered. All animal experiments were performed in compliance with the standards of animal welfare and Ethical Treatment by the Ministry of Science and Technology of China and approved by the Committee on Ethical Use of Animals of Air Force Medical University.

2.14. Immunofluorescence

Frozen tissue sections were fixed with acetone for 30 min. For immunofluorescence, the following primary antibodies were used: VEGFA, CAS3, P53, CCND1, and F4/80. The following reagents were used: Alexa Fluor 488-anti fluorescein, Alexa Fluor 594, and DAPI. All antibodies were diluted in TBST before being applied to tissue sections. Primary antibody incubations (12–14 h at 4 °C) were washed three times with PBS for 5 min. Secondary antibody incubations (30 min at room temperature) were washed three times with PBS for 5 min. After the final wash in PBS, the sections were visualized using a Leica DMRE microscope. Sections were analyzed sequentially using 350 nm (blue), 470–490 nm (green), and 515–600 nm (red) excitation filters and photographed using a Leica camera. Sequential images were processed and superimposed using Adobe Photoshop version 7.0.

2.15. Transwell analysis

According to the method previously reported [32,33], a transwell analysis was performed by using 24 mm transwell tissue culture-treated inserts with 8.0 μM pore size polyester membranes (3428, Corning). Then, 2 × 10^5, 3 × 10^5, 4 × 10^5 human breast cancer cell MDA-MB-453 were seeded in 2 mL DMEM HIGH/GLUCOSE on the bottom of polyester membranes. After 24 h, 5 × 10^5 Mφ and AE-Mφ were added in 2 mL DMEM HIGH/GLUCOSE on the top of polyester membranes. After 24 h, the cells on the upper layer of the polyester membrane with a cotton swab were wiped gently, then dye them with crystal violet staining solution (solarbo) for 10 min, the membrane was washed with PBS for three times, and taken photos with microscope. The crystal violet embedded in polyester membranes was eluted with 33% acetic acid and determined quantitatively by Microplate reader.

2.16. Statistical analysis

Data analysis was conducted with the SPSS 23.0 (SPSS, Chicago, IL, USA) by ANOVA, and all data in our research were considered statistically significant when P value<0.05.

3. Results and discussion

3.1. Construction and characterization of affibody-armed macrophages

Given the importance of HER2 as a therapeutic target for the treatment of breast cancer [34], we genetically engineered RAW264.7 cells to stably express an anti-HER2 affibody on the exterior of the cellular membrane through lentiviral (LV) infection, resulting in AE-Mφ. Scheme 1 schematically depict the preparative steps of AE-Mφ. Briefly, green fluorescent protein (GFP) was anchored onto the macrophage membrane to produce GFP-expressing macrophages (AE-Mφ). Confocal laser scanning microscopy (CLSM) could easily detect the expression of GFP fusion protein on the cell membrane of both HEK 293 T and RAW264.7 macrophages (Mφ) (Fig. 1A). As predicted, anti-HER2 affibody was consistently expressed on the exterior of macrophages. Quantitative PCR and western blotting provided additional evidence to support this conclusion (Fig. 1B and C). Furthermore, flow cytometry was performed to determine whether the affibody visible on the outside of macrophages still had bioactivity. AE-Mφ were treated with a commercial HER2 recombinant protein labeled with phycoerythrin (PE). RAW264.7 cells were used as controls. As seen in Fig. 1D, the addition of an affibody significantly improved the ability of Mφ to bind to HER2, providing additional proof of the successful fabrication of AE-Mφ. CLSM pictures (Fig. 1E) indicated that PE-labeled HER2 protein was mostly localized at the membranes of AE-Mφ, consistent with the data of flow cytometry experiments. Co-immunoprecipitation (Co-IP) was performed using a commercial resin column and an anti-GFP antibody to further confirm the connection between AE-Mφ and HER2 (Fig. 1F). After AE-Mφ was incubated with HER2, the input sample was used as a positive control to find an anti-HER2 band, and the Co-IP products were tested using an immunoblotting technique. Fig. 1G shows that the eluent products of AE-Mφ immunoprecipitated alongside anti-GFP, demonstrating the direct contact between AE-Mφ and the anti-GFP antibody in the commercial resin column. This interaction further demonstrated the binding ability of the expressed affinity to HER2. Collectively, our findings showed that the anti-HER2 affibody was successfully expressed on the macrophage membrane, which was necessary for improving the tumor-targeting ability of macrophage-based delivery systems. Based on the previous reports [16,35], we construct the NPs(DOX) with PLGA (Fig. 1H). Furthermore, NPs(DOX)-loaded AE-Mφ was obtained for following analysis in present work (Fig. 1I).

3.2. In vitro performance evaluation of anti-tumor effect on affibody-armed macrophages and drug delivery is designed to enhance the efficacy of cell therapy

We assessed the anti-tumor effects of AE-Mφ after demonstrating the strong HER2-binding capacity. The in vitro measurement of AE-Mφ induced cytotoxicity was carried out using the real-time cell electronic sensing (RT-CES) technology. An E-Plate 16 was used to measure the electrical impedance across the bottom of each well, and an increase in electrical impedance served as a direct cell index in this method [36]. Real-time cell growth curves were obtained at various effector-to-tumor (E:T) ratios. As shown in Fig. 2A, the anti-tumor effects of AE-Mφ on MDA-MB-453 ($HER2^+$) cells increased as the E:T ratio increased and E:T ratio of 1:1 resulted in the greatest reduction in MDA-MB-453 growth. The release of lactate dehydrogenase (LDH) [37] was determined to assess the cytolytic activity of AE-Mφ and macrophages against MDA-MB-453 cells at various E:T ratios to further validate the observed anti-tumor action caused by armed extracellular affibody. As shown in Fig. 2B, AE-Mφ might provide more cytotoxic effects than macrophages at the same E:T ratio approached 1:1. Additionally, the macrophage phagocytosis assay revealed no discernible difference between the macrophage and AE-Mφ groups in terms of phagocytosis (Fig. 2C and D), indicating that the armed affibody played a substantial role in the increased cytotoxicity of AE-Mφ. Subsequently, we used cytochalasin B (CB) to block phagocytosis of Mφ and AE-Mφ respectively, and then added MDA-MB-453 tumor cells. Flow cytometry was used to detect the ability of Mφ + CB and AE-Mφ + CB groups to phagocytose tumor cells. The results showed that after macrophages were treated with CB, both Mφ and AE-Mφ lost the function of phagocytosis of tumors (Fig. S1), which suggested that one of the important anti-tumor mechanisms of AE-Mφ is derived from phagocytosis of macrophages. Next, we explored

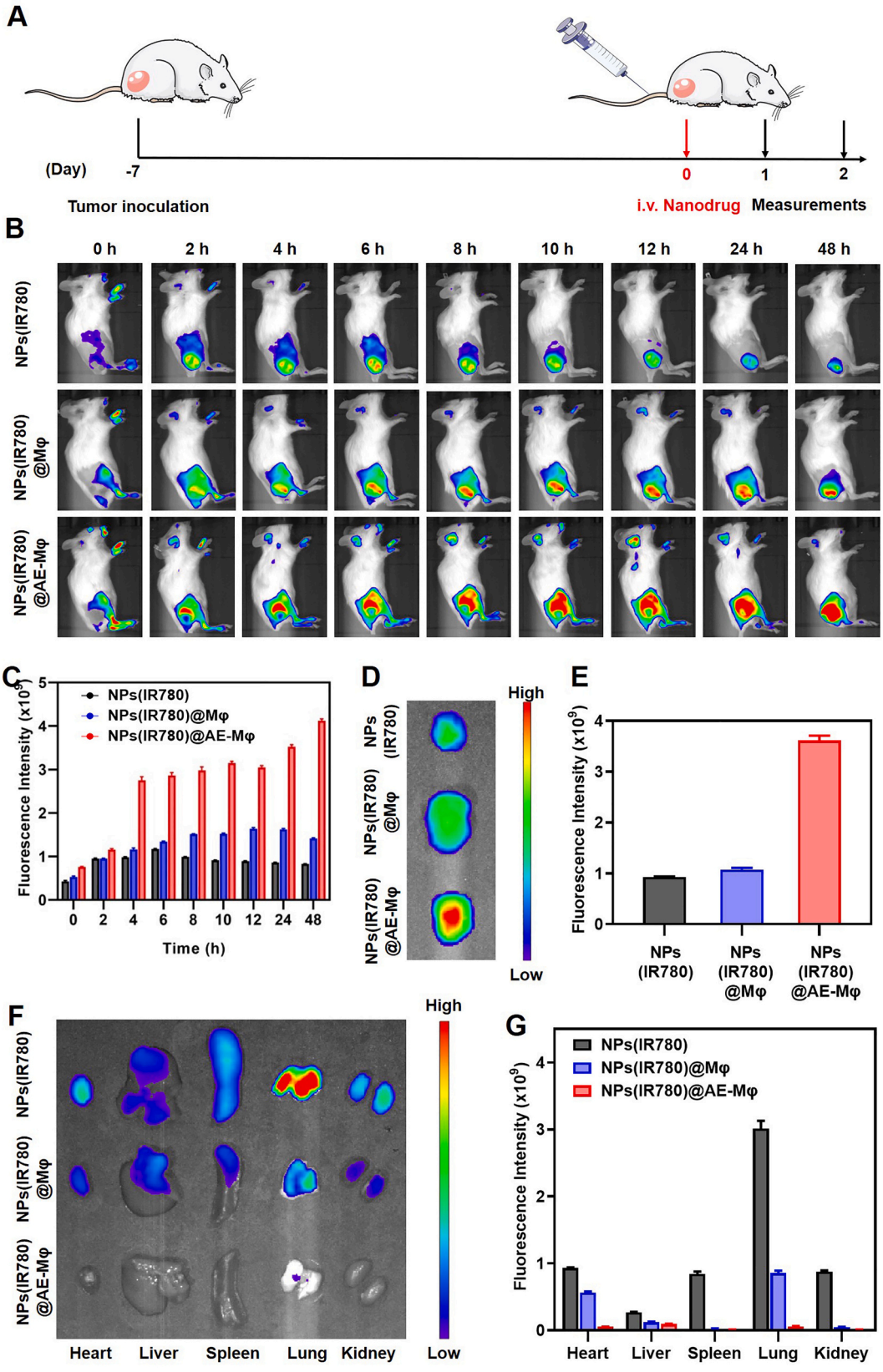

Fig. 3. Significantly enhanced tumor-targeting of affibody-armed macrophages in vitro and in vivo. (A) The Her2^{+}-4 T1 breast cancer model was constructed. Tumor-bearing mice were injected i.v. with NPs(IR780)@AE-Mφ, NPs(IR780)@Mφ and NPs(IR780), and tracked by IVIS spectrum in vivo imaging system. (B) In vivo fluorescence imaging of IR820@ZIF-8, MBP and AMBP NPs in HER2^{+}-4 T1 tumor-bearing mice. (C) The fluorescence intensity within the tumor region after different treatments. (D) Ex vivo fluorescence images of tumor. (E) The fluorescence intensity within the tumor region after different treatments. (F) Ex vivo fluorescence images of major organs (heart, liver, spleen, lung, kidney). (G) The Fluorescence intensity within the heart, liver, spleen, lung, kidney region after different treatments. The opposite phenomenon was observed on fluorescence signals distributed in major organs. Their quantitative analysis by using imageJ was gained.

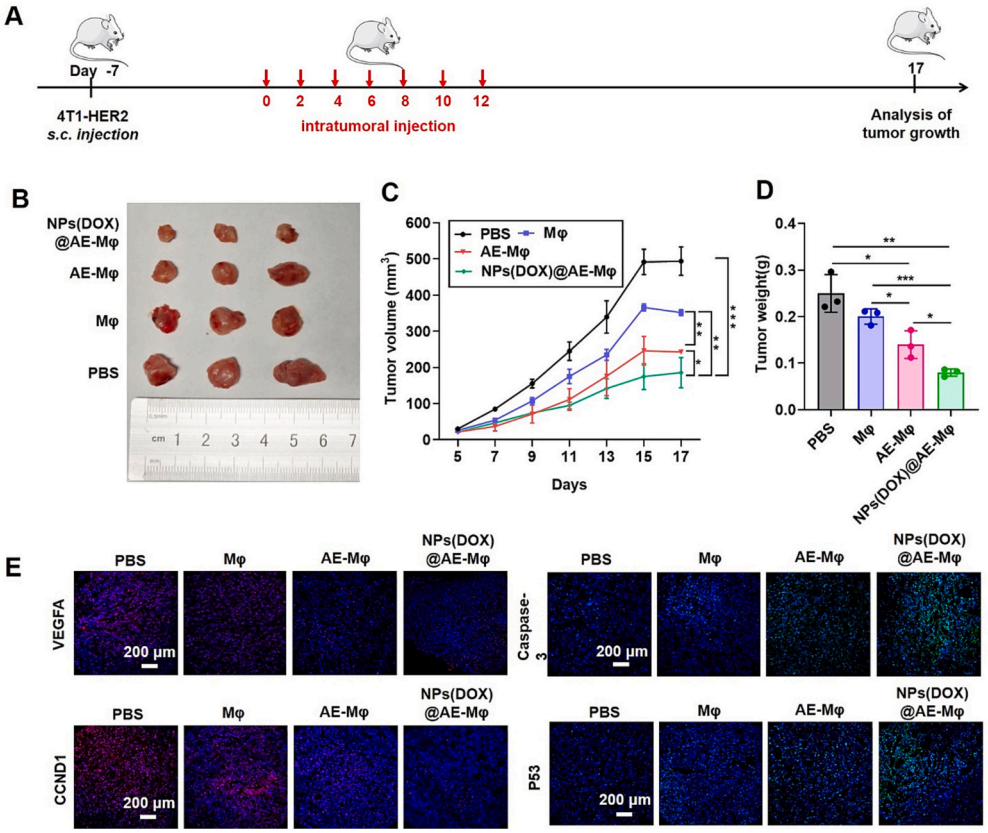

Fig. 4. Drug-loading affibody-armed macrophage exhibited more enhanced anti-tumor efficacy than conventional therapy strategies. (A) BALB/c mice were subcutaneously implanted with HER2 + -4 T1 cells and treated with different treatment groups (NPs(DOX)@AE-Mφ, AE-Mφ, Mφ) and PBS as the control. (B) The analysis of photograph of tumors was compared on tumor inhibition in different groups in HER2 + -4 T1 breast cancer models with caudal vein administration. (C) The analysis of tumor volume was compared on tumor inhibition in different groups. (D) The analysis of tumor weight was compared on tumor inhibition in different groups. (E) Immunofluorescence analysis on specific protein expression of tumor tissue was carried out, in which CAS3 and P53 were significantly upregulated while VEFGA and CCND1 were significantly downregulated. Error bars represent SD, $n = 3$, $^{*}P < 0.05$, $^{**}P < 0.01$, $^{***}P < 0.001$.

the killing effect based on the affibody design. Mφ and AE-Mφ were block phagocytosis ability with CB respectively, then to kill MDA-MB-453 tumor cells. We detected changes on the expression of key downstream effector genes (*p53*, *Caspase-3*, *CCND-1* and *Ki67*) associated with HER2 signaling pathway by qPCR. The results indicate that the expression level of the *p53* (Fig. 2E) and *Caspase-3* (Fig. 2F) were increased over time whereas *CCND-1* was attenuated (Fig. 2G). Cell proliferation was significantly inhibited, such as a significant down-regulation of *Ki67* (Fig. 2H). Therefore, one of the important anti-tumor mechanisms of AE-Mφ is derived from the effect of affibody on blocking the HER2 signaling pathway in tumor cells. These findings demonstrated that AE-Mφ had a considerably enhanced anti-tumor effect in vitro based on armed affibody. It has been well known that macrophages can naturally migrate to sites of malignancy on account of immune cell recruitment feature. A transwell assay in vitro was employed to access different migrating ability to MDA-MB-453 cells between AE-Mφ group and Mφ group (Fig. S2). Mφ exhibited their adoptively transferred characteristics to MDA-MB-453 cells with a dose-dependent relationship. Interestingly, AE-Mφ exhibited concentration dependent migration towards MDA-MB-453 cells about three-fold greater than those of Mφ in vitro migration assay.

We then evaluated the therapeutic effectiveness of NPs(DOX)-loaded AE-Mφ at the cellular level. According to a recent study, DOX can be loaded into RAW264.7 cells to retain excellent cell viability for at least 24 h before completing rapid and precise transport into cancer cells by the tunneling nanotubular highway [38]. DOX was first loaded onto PLGA nanoparticles (NPs(DOX)) (Fig. S3), which were then incubated with AE-Mφ or RAW264.7 cells to produce NPs(DOX)@AE-Mφ and NPs (DOX)@Mφ, respectively. The intrinsic phagocytic capacity of the macrophages allowed them to engulf NPs(DOX) or free DOX in a time-dependent manner, as shown in CLSM images in Fig. S4. However, NPs(DOX) were more effectively absorbed by macrophages than DOX and showed greater intracellular fluorescence signals. Notably, NPs (DOX) showed low cytotoxicity towards macrophages compared to free DOX (Fig. S5). Finally, we determined that the safe concentration of NPs (DOX) for subsequent investigations was 4 μg/mL DOX. NPs(DOX) demonstrated remarkable anti-tumor activity towards MDA-MB-453 cells, as revealed by RT-CES analysis at E:T ratios of 1:1 (Fig. 2I), which was supported by the cytotoxicity results determined by the Cell Counting Kit-8 (CCK-8) assay [39] (Fig. 2J). This was in contrast to their good compatibility with macrophages. Notably, at an E:T ratio of 1:1, the NPs(DOX)@AE-Mφ group had a considerably improved anti-tumor impact compared to the NPs(DOX) or NPs(DOX)@Mφ groups, demonstrating the interaction between cell treatment and targeted chemotherapy. NPs(DOX)@AE-Mφ might act synergistically to increase the death of cancer cells.

3.3. Significantly enhanced tumor-targeting of affibody-armed macrophages in vivo

Macrophages as immune cells can move spontaneously to areas of cancer [40,41]. Therefore, we examined the potential of AE-Mφ as a breast tumor target in vivo. As a pharmacological model, PLGA was loaded with the near-infrared dye IR780, named as NPs(IR780). NPs (IR780), NPs(IR780)@Mφ, and NPs(IR780)@AE-Mφ were intravenously injected via the tail into $HER2^{+}$-4 T1 (built by our lab) tumor-bearing

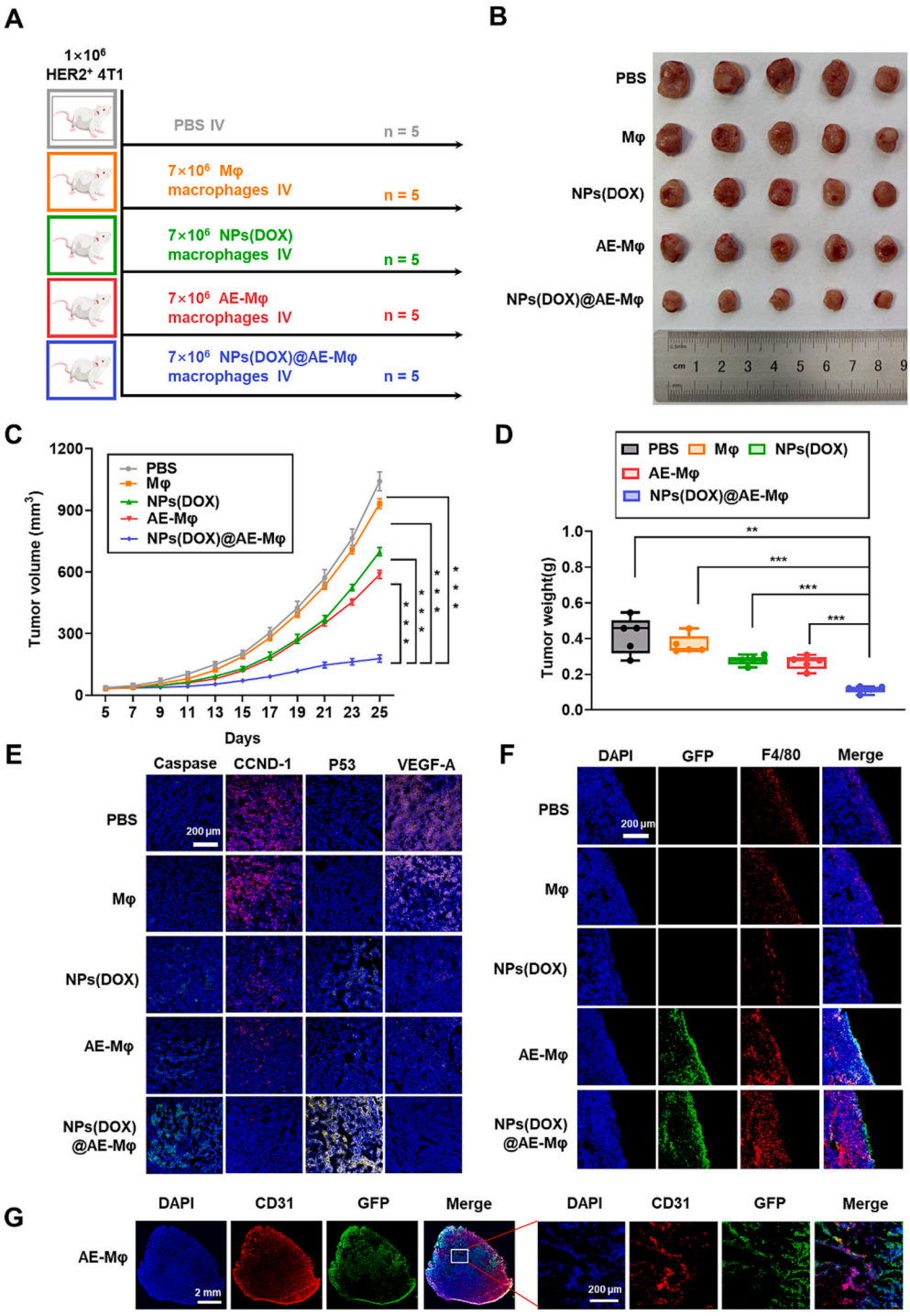

Fig. 5. Caudal vein administration demonstrated significant therapeutic benefit to drug-loading affibody-armed macrophages. (A) Female BALB/c mice were subcutaneously implanted with HER2^{+}-4 T1 cells and treated with different treatment groups or PBS as the control. (B) The analysis of photograph of tumors was compared on tumor inhibition in different groups in HER2 + -4 T1 breast cancer models with caudal vein administration. (C) The analysis of tumor volume was compared on tumor inhibition in different groups. (D) The analysis of tumor weight was compared on tumor inhibition in different groups. (E) Changes were shown by immunofluorescence analysis on the levels of cytokines related to tumor progression in the tumor tissue, including CAS3, P53, VEFGA and CCND1, in which CAS3 and P53 were significantly upregulated while VEFGA and CCND1 were significantly downregulated. (F) Affibody-armed macrophages was significantly enriched in solid tumors than those of ordinary macrophages. (G) AE-Mφ can free from blood vessels and infiltrate deep into solid tumors. Error bars represent SD, $n = 5$, $^{*}P < 0.05$, $^{**}P < 0.01$, $^{***}P < 0.001$.

mice. The living animals were examined using an in vivo imaging system (IVIS) (Fig. 3A). Fluorescence at the tumor site of the mice given NPs (IR780)@AE-Mφ injections gradually increased within 48 h and reached the highest at 48 h (Fig. 3B), indicating effective enrichment of NPs (IR780)@AE-Mφ in tumor tissue, despite the fact that all three groups produced obvious fluorescence signals in the tumor. This enrichment was most likely caused by increased tumor-targeting by the affibody, which allowed for higher fluorescence intensity compared to the other groups (Fig. 3C). Ex vivo imaging of the tumors and major organs removed from mice euthanized post-injection also confirmed the

excellent tumor-targeting of NPs(IR780)@AE-Mφ (Fig. 3D and F). According to further quantitative examination of the average fluorescence intensity from tumors, there was an approximately 4-fold concentration of NPs(IR780)@AE-Mφ at the tumor site compared to that in the other control groups (Fig. 3E and G), consistent with the in vivo imaging data. There is a possible mechanism. On the one hand, NPs(IR780) have been loaded into AE-Mφ as living cell drug carriers, which reduced IR780 released into tissues when they entered the circulation in vivo. On the other hand, the increased targeting of AE-Mφ augmented the IR780 enrichment into tumor sites. Collectively, these findings show the potential of the AE-Mφ technology for precise drug administration, allowing increased medication concentration at the tumor location.

3.4. Live drug delivery contributes to boost the efficacy of cell therapy based on high tumor-targeting of affibody-armed macrophages

We confirmed the therapeutic effectiveness of NPs(DOX)@AE-Mφ in $HER2^{+}$-4 T1 subcutaneous tumor model after demonstrating the potential of this compound for targeted DOX administration and synergistic anti-tumor action in vitro. To perform anti-tumor studies in animals, a $HER2^{+}$-4 T1 subcutaneous tumor model was developed. This was performed because MDA-MB-453 cells have low tumorigenicity when used as cell-derived xenografts in BALB/c mice. Peritumoral injection was used as an initial trial to reduce systemic differences. In mice treated with NPs(DOX)@AE-Mφ as opposed to animals treated with AE-Mφ, $HER2^{+}$-4 T1 tumor development was considerably suppressed, according to multiple group analysis (Fig. 4A-D). When the NPs(DOX)@AE-Mφ group was compared with the control group, immunofluorescence examination of the tumor tissue showed that P53 and CAS3 were dramatically elevated, whereas cyclin D1 (CCND1) and vascular endothelial growth factor A (VEGFA) were significantly downregulated (Fig. 4E).

NPs(DOX)@AE-Mφ and control groups AE-Mφ, NPs(DOX), Mφ, and PBS were independently injected into the tail vein of tumor-bearing BALB/c nude mice ($n = 5$ per group) to better simulate the administration route of clinical live cell treatment (Fig. 5A). NPs(DOX)@AE-Mφ resulted in a significant inhibition of tumor growth as opposed to the constant tumor growth seen in the other groups of mice (Fig. 5B-D), firmly establishing the competence of the NPs(DOX)@AE-Mφ for highly specific treatment of breast cancer through the integration of chemotherapy with affibody-mediated cell therapy. Immunofluorescence study of tumor tissue, which showed that affibody-armed macrophages was substantially enriched in solid tumors than those of conventional macrophages, provided additional evidence of the excellent anti-cancer activity of NPs(DOX)@AE-Mφ. We also assessed the expression of genes, including such as P53, CAS3, CCND1 and VEGFA, which are involved in cancer cell proliferation, death, and the cell cycle. Fig. 5E demonstrates that when the NPs(DOX)@AE-Mφ was administered, P53 and CAS3 were significantly upregulated compared with the control groups, while VEGFA and CCND1 were significantly downregulated, indicating that the development of tumor tissue is inhibited by regulating apoptosis and cell cycle. Analysis of the groups that received peritumoral injections supported this finding (Fig. 4). Mice injected with NPs(DOX)@AE-Mφ showed no evident body weight loss or aberrant behavior, indicating insignificant adverse effects (Fig. S6). Meanwhile, the H&E staining results of main organs (heart, liver, spleen, lung, and kidney) in the NPs(DOX)@AE-Mφ group showed good biosafety (Fig. S7).

In this study, we found that considerable tumor suppression occurred after two caudal vein administrations. However, significant tumor suppression may also occur after seven peritumoral administrations. We believe that this effect results from blood circulation being more suited to maintaining macrophage viability and enhancing deep tumor penetration. When combined with precise targeting, AE-Mφ, which is a live cell drug carrier, makes it easier for solid tumors to become enriched. The enrichment of AE-Mφ was substantially higher than that in the normal macrophages (Fig. 5F), whereas AE-Mφ may infiltrate deeply into solid tumors while remaining free of blood vessels, the tumors were primarily interstitial areas devoid of blood vessels (Fig. 5G). This might help explain how AE-Mφ medication delivery produces impressive therapeutic results. According to this study, live cell drug delivery provided therapeutic benefits when administered intravenously. Moreover, it can aggressively target solid tumors, efficiently enhance drug delivery, and ultimately produce acceptable therapeutic outcomes.

4. Conclusion

We created NPs(DOX)@AE-Mφ, a live macrophages-based therapeutic system that may work in concert to greatly increase anti-tumor effectiveness by selectively targeting HER2. We genetically modified macrophages to directly produce anti-HER2 antibodies on their extracellular membrane, rather than utilizing post-functionalization techniques. Our in vitro findings showed that extracellular macrophages equipped with affibodies effectively retained their bioactivities, resulting in NPs(DOX)@AE-Mφ with outstanding HER2-targeting potential, as well as affibody-mediated anti-tumor activity. In addition to significantly increasing the accumulation of DOX at the tumor site for targeted chemotherapy, NPs(DOX)@AE-Mφ also displayed a considerable synergistic effect in combination with DOX/anti-HER2 treatments compared to the un-engineered equivalents. Consequently, $HER2^{+}$ breast tumor development was successfully prevented. Our study offers a solid plan for creating therapeutic platforms based on macrophages, which are highly targeted for breast cancer treatment. This approach may also be used to treat other cancers and disorders by adding other bioactive compounds to the macrophage surface.

CRediT authorship contribution statement

Pengbo Ning: Writing – review & editing, Project administration, Investigation, Funding acquisition, Formal analysis, Data curation, Conceptualization. **Fuyu Du:** Investigation, Data curation. **Haotian Wang:** Validation, Resources, Formal analysis. **Xiaocheng Gong:** Data curation, Conceptualization. **Yuqiong Xia:** Formal analysis. **Xianghan Zhang:** Visualization, Validation. **Hongzhang Deng:** Validation. **Ruili Zhang:** Writing – original draft, Validation, Investigation, Formal analysis. **Zhongliang Wang:** Writing – review & editing, Supervision, Project administration, Investigation, Conceptualization.

Declaration of competing interest

All authors declare that they have no conflicts of interest and no competing interest.

Data availability

No data was used for the research described in the article.

Acknowledgements

This work was supported by the National Natural Science Foundation of China (32071406, 31470535, and 82272159), Key Research and Development Projects of Shaanxi Province (2023-ZDLSF-18), the Key R & D program of Xianyang City (2021ZDYF-SF-0023), Innovation Capability Support Program of Shaanxi (Program No. 2022TD-52), Guang-Dong Basic and Applied Basic Research Foundation (2023A1515030207). We thank Ms. Min Liu and Mr. Hongyu Fan for their excellent technical assistance. We acknowledge the Instrumental Analysis Center of Xidian University for providing test equipment.

Appendix A. Supplementary data

Supplementary data to this article can be found online at https://doi.org/10.1016/j.jconrel.2024.02.003.

References

[1] T. Hou, T. Wang, W. Mu, R. Yang, S. Liang, Z. Zhang, S. Fu, T. Gao, Y. Liu, N. Zhang, Nanoparticle-loaded polarized-macrophages for enhanced tumor targeting and cell-chemotherapy, Nano Lett. 13 (2020) 6.

[2] W. Zhang, M. Wang, W. Tang, R. Wen, S. Zhou, C. Lee, H. Wang, W. Jiang, I. M. Delahunty, Z. Zhen, H. Chen, M. Chapman, Z. Wu, E.W. Howerth, H. Cai, Z. Li, J. Xie, Nanoparticle-laden macrophages for tumor-tropic drug delivery, Adv. Mater. 34 (2022) e2109925.

[3] D. Rosenblum, N. Joshi, W. Tao, J.M. Karp, D. Peer, Progress and challenges towards targeted delivery of cancer therapeutics, Nat. Commun. 9 (2018) 1410.

[4] F. Combes, E. Meyer, N.N. Sanders, Immune cells as tumor drug delivery vehicles, J. Control. Release 327 (2020) 70–87.

[5] T. Xiao, W. Hu, Y. Fan, M. Shen, X. Shi, Macrophage-mediated tumor homing of hyaluronic acid nanogels loaded with polypyrrole and anticancer drug for targeted combinational photothermo-chemotherapy, Theranostics 11 (2021) 7057–7071.

[6] J.K. Patra, G. Das, L.F. Fraceto, E.V.R. Campos, M.D.P. Rodriguez-Torres, L. S. Acosta-Torres, L.A. Diaz-Torres, R. Grillo, M.K. Swamy, S. Sharma, S. Habtemariam, H.S. Shin, Nano based drug delivery systems: recent developments and future prospects, J. Nanobiotechnol. 16 (2018) 71.

[7] C. Zhao, X. Pang, Z. Yang, S. Wang, H. Deng, X. Chen, Nanomaterials targeting tumor associated macrophages for cancer immunotherapy, J. Control. Release 341 (2022) 272–284.

[8] N. Liang, N. Ren, Z. Feng, Z. Sun, M. Dong, W. Wang, F. Liu, C. Sun, W. Zhou, Z. Xing, J. Wang, C. Liu, H. Liu, Biomimetic metal-organic frameworks as targeted vehicles to enhance osteogenesis, Adv. Healthc. Mater. 11 (2022) e2102821.

[9] H. Wu, T. Zhang, N. Li, J. Gao, Cell membrane-based biomimetic vehicles for effective central nervous system target delivery: insights and challenges, J. Control. Release 360 (2023) 169–184.

[10] N. Khosravi, E. Pishavar, B. Baradaran, F. Oroojalian, A. Mokhtarzadeh, Stem cell membrane, stem cell-derived exosomes and hybrid stem cell camouflaged nanoparticles: a promising biomimetic nanoplatforms for cancer theranostics, J. Control. Release 348 (2022) 706–722.

[11] Y. Miao, Y. Yang, L. Guo, M. Chen, X. Zhou, Y. Zhao, D. Nie, Y. Gan, X. Zhang, Cell membrane-camouflaged nanocarriers with biomimetic deformability of erythrocytes for ultralong circulation and enhanced cancer therapy, ACS Nano 16 (2022) 6527–6540.

[12] W. Lei, C. Yang, Y. Wu, G. Ru, X. He, X. Tong, S. Wang, Nanocarriers surface engineered with cell membranes for cancer targeted chemotherapy, J. Nanobiotechnol. 20 (2022) 45.

[13] R. Noy, J.W. Pollard, Tumor-associated macrophages: from mechanisms to therapy, Immunity 41 (2014) 49–61.

[14] K. Ying, Y. Zhu, J. Wan, C. Zhan, Y. Wang, B. Xie, P. Xu, H. Pan, H. Wang, Macrophage membrane-biomimetic adhesive polycaprolactone nanocamptothecin for improving cancer-targeting efficiency and impairing metastasis, Bioact. Mater. 20 (2023) 449–462.

[15] Y. Xia, L. Rao, H. Yao, Z. Wang, P. Ning, X. Chen, Engineering macrophages for cancer immunotherapy and drug delivery, Adv. Mater. 32 (2020) e2002054.

[16] Z. Rao, C. Lu, H. Fan, F. Du, Y. Zhu, Y. Xia, Z. Wang, P. Ning, Engineered macrophages-based uPA-scavenger load gemcitabine to prompt robust treating cancer metastasis, Adv. Healthc. Mater. 12 (2023) e2203356.

[17] Q. Lu, T. Liu, Z. Han, J. Zhao, X. Fan, H. Wang, J. Song, H. Ye, J. Sun, Revolutionizing cancer treatment: the power of cell-based drug delivery systems, J. Control. Release 361 (2023) 604–620.

[18] P.Y. Li, Z. Fan, H. Cheng, Cell membrane bioconjugation and membrane-derived nanomaterials for immunotherapy, Bioconjug. Chem. 29 (2018) 624–634.

[19] A.R. Jalil, M.P. Tobin, D.E. Discher, Suppressing or enhancing macrophage engulfment through the use of CD47 and related peptides, Bioconjug. Chem. 33 (2022) 1989–1995.

[20] H. Hong, O.J. Lee, Y.J. Lee, J.S. Lee, O. Ajiteru, H. Lee, Y.J. Suh, M.T. Sultan, S. H. Kim, C.H. Park, Cytocompatibility of modified silk fibroin with glycidyl methacrylate for tissue engineering and biomedical applications, Biomolecules 11 (1) (2020) 35.

[21] P. Shi, Y. Wang, Synthetic DNA for cell-surface engineering, Angew. Chem. Int. Ed. Eng. 60 (2021) 11580–11591.

[22] M. Ovais, M. Guo, C. Chen, Tailoring nanomaterials for targeting tumor-associated macrophages, Adv. Mater. 31 (2019) e1808303.

[23] D.B. Cox, R.J. Platt, F. Zhang, Therapeutic genome editing: prospects and challenges, Nat. Med. 21 (2015) 121–131.

[24] S.W. Wang, C. Gao, Y.M. Zheng, L. Yi, J.C. Lu, X.Y. Huang, J.B. Cai, P.F. Zhang, Y. H. Cui, A.W. Ke, Current applications and future perspective of CRISPR/Cas9 gene editing in cancer, Mol. Cancer 21 (2022) 57.

[25] N. Zhao, Y. Song, X. Xie, Z. Zhu, C. Duan, C. Nong, H. Wang, R. Bao, Synthetic biology-inspired cell engineering in diagnosis, treatment, and drug development, Signal Transduct. Target. Ther. 8 (2023) 112.

[26] X. Yan, X. Liu, C. Zhao, G.Q. Chen, Applications of synthetic biology in medical and pharmaceutical fields, Signal Transduct. Target. Ther. 8 (2023) 199.

[27] X. Deng, Z. Shao, Y. Zhao, Solutions to the drawbacks of Photothermal and photodynamic Cancer therapy, Adv. Sci. (Weinh) 8 (2021) 2002504.

[28] G. Tiscornia, O. Singer, I.M. Verma, Production and purification of lentiviral vectors, Nat. Protoc. 1 (2006) 241–245.

[29] R. Deng, Y. Wang, L. Yang, C.D. Bain, In situ fabrication of polymeric microcapsules by ink-jet printing of emulsions, ACS Appl. Mater. Interfaces 11 (2019) 40652–40661.

[30] J. Tian, H. Cao, W. Wu, Q. Yu, N.P. Guisinger, Y.P. Chen, Graphene induced surface reconstruction of cu, Nano Lett. 12 (2012) 3893–3899.

[31] H. Ye, K. Wang, M. Wang, R. Liu, H. Song, N. Li, Q. Lu, W. Zhang, Y. Du, W. Yang, L. Zhong, Y. Wang, B. Yu, H. Wang, Q. Kan, H. Zhang, Y. Wang, Z. He, J. Sun, Bioinspired nanoplatelets for chemo-photothermal therapy of breast cancer metastasis inhibition, Biomaterials 206 (2019) 1–12.

[32] P. Li, C. Wang, J. Qiu, F. Song, Y. Huang, Y. Zhang, K. Zhang, H. Ji, Y. Sang, J. J. Blaker, Y. Zhang, L. Han, Inhibitory effect of zinc oxide nanorod arrays on breast cancer cells profiled through real-time cytokines screening by a single-cell microfluidic platform, BMEMat 1 (2023) e12040.

[33] I. Shabo, K. Midtbo, H. Andersson, E. Akerlund, H. Olsson, P. Wegman, C. Gunnarsson, A. Lindstrom, Macrophage traits in cancer cells are induced by macrophage-cancer cell fusion and cannot be explained by cellular interaction, BMC Cancer 15 (2015) 922.

[34] E.A. Perez, C. Dang, C. Lee, J. Singh, K. Wang, J.B. Layton, A. Gilsenan, M. D. Hackshaw, J. Cortes, Incidence of adverse events with therapies targeting HER2-positive metastatic breast cancer: a literature review, Breast Cancer Res. Treat. 194 (2022) 1–11.

[35] Y. Zhang, Y. Chen, C. Lo, J. Zhuang, P. Angsantikul, Q. Zhang, X. Wei, Z. Zhou, M. Obonyo, R.H. Fang, W. Gao, L. Zhang, Inhibition of pathogen adhesion by bacterial outer membrane-coated nanoparticles, Angew. Chem. Int. Ed. Eng. 58 (2019) 11404–11408.

[36] Y. Wang, C. Tong, H. Dai, Z. Wu, X. Han, Y. Guo, D. Chen, J. Wei, D. Ti, Z. Liu, Q. Mei, X. Li, L. Dong, J. Nie, Y. Zhang, W. Han, Low-dose decitabine priming endows CAR T cells with enhanced and persistent antitumour potential via epigenetic reprogramming, Nat. Commun. 12 (2021) 409.

[37] A. Jo, J.H. Bae, Y.J. Yoon, T.H. Chung, E.W. Lee, Y.H. Kim, H.M. Joh, J.W. Chung, Plasma-activated medium induces ferroptosis by depleting FSP1 in human lung cancer cells, Cell Death Dis. 13 (2022) 212.

[38] L. Guo, Y. Zhang, Z. Yang, H. Peng, R. Wei, C. Wang, M. Feng, Tunneling nanotubular expressways for ultrafast and accurate M1 macrophage delivery of anticancer drugs to metastatic ovarian carcinoma, ACS Nano 13 (2019) 1078–1096.

[39] X. Jiang, X. Huang, G. Zheng, G. Jia, Z. Li, X. Ding, L. Lei, L. Yuan, S. Xu, N. Gao, Targeting PI4KA sensitizes refractory leukemia to chemotherapy by modulating the ERK/AMPK/OXPHOS axis, Theranostics 12 (2022) 6972–6988.

[40] L. Cassetta, J.W. Pollard, A timeline of tumour-associated macrophage biology, Nat. Rev. Cancer 23 (2023) 238–257.

[41] R. Bai, Y. Li, L. Jian, Y. Yang, L. Zhao, M. Wei, The hypoxia-driven crosstalk between tumor and tumor-associated macrophages: mechanisms and clinical treatment strategies, Mol. Cancer 21 (2022) 177.